Avicenna Journal of Phytomedicine (AJP)

Original article

Tinospora crispa attenuates cognitive dysfunction and amyloid–tau pathology in a High-Fat High-Fructose-induced Alzheimer's rat model

Kartika Rahma[1,2], Erni Hernawati Purwaningsih[3,*], Aulanni'am Aulanni'am[4], Yetti Ramli[5], Mitsuyo Kishida[6]

[1]*Doctoral Program in Biomedical Sciences, Faculty of Medicine, Universitas Indonesia, Jakarta 10430, Indonesia*
[2]*Department of Pharmacy, Faculty of Health Science and Technology, Universitas Binawan, Jakarta 13630, Indonesia*
[3]*Department of Medical Pharmacy, Faculty of Medicine, Universitas Indonesia, Jakarta 10430, Indonesia*
[4]*Department of Chemistry, Faculty of Science, Universitas Brawijaya, Malang 65145, Indonesia*
[5]*Department of Neurology, Faculty of Medicine, Universitas Indonesia, Jakarta 10430, Indonesia*
[6]*Graduate School of Science and Technology, Kumamoto University, 2-39-1 Kurokami, Chuo-ku, Kumamoto, 860-8555, Japan*

Article history:
Received: Oct 23, 2025
Received in revised form: Feb 27, 2026
Accepted: Mar 03, 2026
Epub ahead of print

**** Corresponding Author:***
Tel: +62 81311094035
Fax: +62 21 3912477
erni.hernawati@ui.ac.id

Keywords:
Tinospora crispa
Cognitive dysfunction
Amyloid beta
P-Tau
Alzheimer disease

Abstract

Objective: Alzheimer's disease (AD) is characterized by amyloid-β (Aβ) plaques and Tau hyperphosphorylation, processes regulated by key enzymes including β-site amyloid precursor protein-cleaving enzyme 1 (BACE1), presenilin-1 (PSEN1), and glycogen synthase kinase-3β (GSK3β). This pathology is further aggravated by insulin resistance which disrupts neuronal signaling and metabolism. However, current therapies face significant challenges in targeting these interconnected mechanisms simultaneously. This study investigated the modulatory effects of *Tinospora crispa* (L.) Hook.f. & Thomson (*T. crispa*) extract on Aβ deposition, Tau hyperphosphorylation, and cognitive function in an AD-like pathological model induced in insulin-resistant rats.

Materials and methods: Rats were subjected to a high-fat high-fructose (HFHF) diet combined with streptozotocin (STZ) to induce AD-like pathology. Cognitive performance was evaluated using the Y-maze, while Aβ and phosphorylated Tau (p-Tau) were assessed by immunohistochemistry (IHC). *In silico* docking was also performed to evaluate interactions between *T. crispa* compounds and BACE, PSEN1, and GSK3β.

Results: Treatment with *T. crispa* (400 mg/kg) improved spatial memory by 93.5% and reduced Aβ by 49.3% and p-Tau by 36.3%, with greater effects than metformin across all three parameters. Docking revealed strong affinities of borapetoside B for BACE and tinoscorside A for PSEN1 and GSK3β, supporting their multi-target activity in AD pathways.

Conclusion: These findings suggest that *T. crispa* and its active constituents exert multi-target neuroprotective effects by simultaneously modulating amyloidogenic and Tau-related mechanisms. This work advances knowledge by identifying a natural extract with potential to fill a critical therapeutic gap, though further studies are needed to confirm safety, long-term efficacy, and clinical relevance in humans.

Please cite this paper as:
Rahma K, Purwaningsih E.H, Aulanni'am A, Ramli Y, Kishida M. *Tinospora crispa* attenuates cognitive dysfunction and amyloid–tau pathology in a High-Fat High-Fructose-induced Alzheimer's rat model. Avicenna J Phytomed, 2026

Introduction

Alzheimer's disease (AD) is a progressive neurodegenerative condition and the most common cause of dementia worldwide. It is marked by memory loss, cognitive decline, and the abnormal accumulation of Amiloid βeta (Aβ) and hyperphosphorylated Tau in the brain (Knopman et al. 2021). In recent years, increasing attention has been directed to the role of lifestyle and diet in its development. Diets rich in fat and fructose disrupt metabolic balance. Moreover, they impair insulin signaling in the brain, trigger oxidative stress, and promote inflammation (Mietelska-Porowska et al. 2022; Zhao et al. 2022). Together, these changes create conditions that accelerate Aβ deposition and Tau pathology by reinforcing the close connection between metabolic dysfunction and AD (Mietelska-Porowska et al. 2022).

Despite decades of research, there is still no effective cure for AD. Available drugs provide only temporary symptom relief and do not address the underlying disease process. Metformin, a widely used antidiabetic drug, has attracted particular interest because of its reported ability to improve brain insulin signaling, reduce inflammation, and lower Aβ and phospo-Tau (p-Tau) levels (Oliveira et al. 2021). Nevertheless, despite its well-established metabolic efficacy, long-term metformin therapy has been associated with gastrointestinal side effects and vitamin B12 deficiency, raising concerns about tolerability and prolonged use (Nabrdalik et al. 2024; Shurrab and Arafa 2020 Chen et al. 2023; Diakité et al. 2025). These safety concerns emphasize the need for alternative therapies that are both effective and safer for long-term use.

Natural compounds offer a promising path forward, as they often act on multiple disease pathways with fewer side effects. *Tinospora crispa (T. crispa)*, a traditional medicinal plant used across Southeast Asia, possesses well-established antidiabetic, antioxidant, and anti-inflammatory properties (Xu et al. 2017; Zuhri et al. 2022). However, its potential benefits for the brain—particularly in slowing or preventing AD pathology—remain largely unexplored. Given its strong metabolic activity, *T. crispa* may affect Aβ and p-Tau accumulation as well as cognitive function.

This study aimed to investigate the neuroprotective potential of *T. crispa*, both alone and in combination with metformin, in a rat model of High Fat High Fructose (HFHF)-induced AD. By evaluating its effects on Aβ and p-Tau accumulation, oxidative stress, and cognitive function, this work offers fresh insights into the potential of *T. crispa* as a safer, natural therapeutic candidate, either as a stand-alone treatment or as an adjunct to metformin.

Materials and Methods

Preparation of *T. crispa* extract

The stem simplicia of *T. crispa* was confirmed as *Tinospora. crispa* (L.) Hook.f. & Thomson by the Tawangmangu Traditional Health Service Unit, Ministry of Health, Indonesia (certificate number: TL.02.04/D.XI.6?11535.653/2024). A total of 3 kg of dried stems of *T. crispa* was pulverized into powder and extracted through maceration using 70% ethanol (Merck, Darmstadt, Germany) in a 1:3 (w/v) ratio. Each 500 g batch was soaked at room temperature for 24 hr, followed by two successive re-extractions with the same solvent and ratio for 48 and 72 hr. The combined filtrates were concentrated at ±50°C with a rotary evaporator (Eyela, 281208, Tokyo, Japan) to yield a viscous extract.

Animals and housing conditions

Male Wistar rats (*Rattus norvegicus*), 6–8 weeks old (late adolescent to young adult) and weighing 150–200 g, were obtained from CV. Dunia Kaca, Kemuning, Central Java, Indonesia. All subjects were confirmed to be healthy and physically active prior to inclusion. The rats were fed a high-fat high-fructose (HFHF) diet to induce metabolic alterations associated

with accelerated aging. The study protocol was approved by the Health Research Ethics Committee, Faculty of Medicine, Universitas Indonesia (Number: KET-1752/UN2.F1/ETIK/PPM.00.02/2023).
Rats were housed at the IMERI Animal Research Facility in polypropylene cages (50 × 40 × 20 cm, 2–3 rats per cage) with wood-shaving bedding, under controlled conditions (12 hr light/dark cycle, 21–22°C, 60–70% humidity). Standard chow and water were provided *ad libitum*.

Experimental design

Thirty-five rats were acclimatized for seven days with standard chow and water provided *ad libitum*. They were then randomly assigned into two groups: a normal group (N; n = 5), maintained on a standard rodent diet with water *ad libitum* for 16 weeks, and a HFHF group (n = 30), fed an HFHF diet for the same duration (Figure 1). The high-fat diet was prepared by supplementing the standard diet with quail egg yolk at 10% of the total weight, with a daily ration of 10 g. The high-fructose diet was administered by intragastric gavage twice daily, each dose consisting of 825 mg of 55% fructose in 1.5 ml.

After 8 weeks on the HFHF diet, rats were fasted overnight and injected intraperitoneally with a single dose of streptozotocin (STZ, 22 mg/kg body weight (Gunawan et al. 2023)) on day 58. Streptozotocin (CAS 18883-66-4) was purchased from Santa Cruz Biotechnology, Texas, USA. Upon confirmation of insulin resistance, HFHF-fed rats were randomly divided into six treatment groups: HFHF, MET, TC200, TC400, TC200MET, and TC400MET, with five rats in each group (n = 5). Thus, the study was divided into a total of seven groups, as detailed in Table 1. Animals then received their respective oral treatments—metformin (100 mg/kg/day (Kim et. al 2020; Mobasheret et al. 2020; Mohammad et al. 2023), *T. crispa* extract at 200 or 400 mg/kg body weight per day (Ahmad et al. 2015; Firdausa et al. 2020), or the combination of extract and metformin—while continuing on the HFHF regimen, consisting of high-fat diet and fructose administration, for an additional 8 weeks. Animal health was monitored daily, and any rats that died during the study were excluded from further analysis.

Assessment of insulin resistance

Insulin resistance was confirmed prior to treatment allocation by measuring fasting blood glucose (FBG), fasting insulin (FI), and Homeostatic Model Assessment of Insulin Resistance (HOMA-IR), following the protocol established in our previous study (Rahma et al. 2026). This ensured that all animals exhibited comparable insulin resistance before receiving treatment.

Behavioral assay for cognitive performance

The cognitive abilities of the rats were evaluated in three stages. The first assessment was conducted at baseline (day 0) before the study began. The second evaluation took place after 8 weeks of HFHF diet feeding followed by a single dose of STZ, to confirm the development of cognitive and memory deficits. The final assessment of spatial and memory function was performed at the end of the study, after 8 weeks of treatment with the extract (week 16). The maze consists of a black plastic structure with three arms (50 cm long, 32 cm high, and 16 cm wide) arranged at 120° angles. This behavioral test was performed three times: before and after the rats were fed an HFHF diet, and after therapy. Rats were placed at the end of one arm and allowed 10 minutes to freely explore the maze (Akbarizadeh-Mashkani et al. 2025). Entries into all arms were recorded (with valid entry requiring all four paws inside the arm), and spontaneous alternation (SPA) was noted if the rat entered three consecutive arms. SPA percentage was calculated using the following equation (1) (J. Kim et al. 2023; Mohamed et al. 2020):

$$\% SPA = \frac{total\ alternation}{(\ total\ entry - 2)}\ x\ 100 \quad (1)$$

Immunohistochemical analysis of Aβ and p-Tau expression in brain tissue

At the end of the study, rats were anesthetized using ketamine (50mg/kg body weight) and xylazine (5mg/kg body weight), administered intraperitoneally and were then sacrificed for brain collection. The tissue was fixed in 10% neutral buffered formalin, embedded in paraffin, and sectioned coronally at a thickness of 8 µm. Sections were mounted on poly-L-lysine–coated slides, deparaffinized, rehydrated, and processed following protocol of Novolink™ Polymer Detection System kit (Leica Biosystems, Newcastle upon Tyne, UK). Immunostaining was performed using anti-beta amyloid 1–42 monoclonal antibody [mOC64] (Abcam, ab201060, Cambridge, UK) (1:500), or with anti-Tau (phospho T231) monoclonal antibody [EPR2488] (Abcam, ab151559, Cambridge, UK) (1:300). Negative controls were prepared by omitting the primary antibody. After counterstaining, sections were dehydrated, cleared, and mounted. Histological analysis was conducted under a light microscope equipped with an Optilab camera system (Miconos, Indonesia). Images were captured at 400x magnification, and a 100 µm scale bar was applied using the accompanying software. For quantitative assessment of Immunohistochemistry (IHC) staining, ten randomly selected fields per slide were analyzed to ensure representative measurements. The percentage area of Aβ and p-Tau in the hippocampus and cortex was quantified using ImageJ software.

In silico analysis of *T. crispa* compounds with related Aβ and p-Tau target proteins

The interactions between the bioactive compounds of *T. crispa* and the target proteins were evaluated using molecular docking analysis. Five bioactive constituents of *T. crispa*— tinoscorside A, β-sitosterol, borapetoside A, borapetoside B, and makisterone C— were selected for their reported roles in modulating insulin resistance (Zuhri et al. 2022). Their 2D structures were retrieved from PubChem (https://pubchem.ncbi.nlm.nih.gov/) in Structure Data File (SDF) format and subsequently prepared and converted to Protein Data Bank (PDB) format using MarvinSketch 23.11.

Molecular docking was performed on a Windows 10 computer equipped with an Intel® Core™ i5-760 processor and at least 4 GB RAM, using AutoDock 4.2 software. Proteins selected for the docking simulations included BACE (PDB ID: 2VKM), PSEN1 (PDB ID: 6LR4), and GSK3β (PDB ID: 8FF8), since BACE and PSEN1 play key roles in the production of amyloid-β plaques (Gene at al. 2022; Hajdú et al. 2023), whereas GSK3β overexpression leads to Tau hyperphosphorylation (Chakraborty et al. 2024). Metformin was used as a positive control for its known effects on brain insulin resistance, Tau pathology, and cognitive deficits in Alzheimer's models (Oliveira et al. 2021). The 3D structures in PDB format were downloaded from the RCSB PDB (https://www.rcsb.org/). The active sites of the proteins, defined by their native ligands, were identified as BSD, ESF, and XFV0 for each respective protein according to the Research Collaboratory for Structural Bioinformatics (RCSB) database.

Proteins were prepared by removing water molecules, adding hydrogens, and assigning Gasteiger charges. Co-crystallized ligands were then separated from the protein structures. For docking, the most complete protein chain was selected.

Docking simulations were performed within an optimized grid box aligned with the coordinates of the co-crystallized ligand to ensure correct binding site orientation. Subsequently, the grid box dimensions were further refined along the x-, y-, and z-axes for each protein, and the configuration

exhibiting the lowest binding energy was selected for further analysis. Test ligands were docked in the optimized grid, and binding affinities (ΔG) were calculated. More negative ΔG values indicated stronger and more spontaneous interactions. Docking visualization and residue mapping were conducted using AutoDock 4.2, while protein–ligand interactions were further analyzed using the Protein–Ligand Interaction Profiler (PLIP; https://plip-tool.biotec.tu-dresden.de/), which provided detailed visualizations and tabulated interaction data.

Statistical analysis

Statistical analyses were conducted using GraphPad Prism version 10.4.0. Results are presented as mean ± standard deviation (SD). Data distribution and homogeneity of variance were assessed using the Shapiro–Wilk and Levene tests to determine the appropriate statistical approach. For normally distributed data with equal variances, one-way ANOVA was performed, followed by Tukey's post hoc tests. The correlations were analyzed using Pearson's correlation test. Descriptive analysis is presented in Tables, graphical or scatter plots formats. Statistical significance was defined as $^{\#\#}p<0.001$ and $^{\#\#\#}p<0.0001$ vs. the N group; $^{\S}p<0.05$, $^{*}p<0.01$, $^{**}p<0.001$, and $^{***}p<0.0001$ vs. the HFHF group.

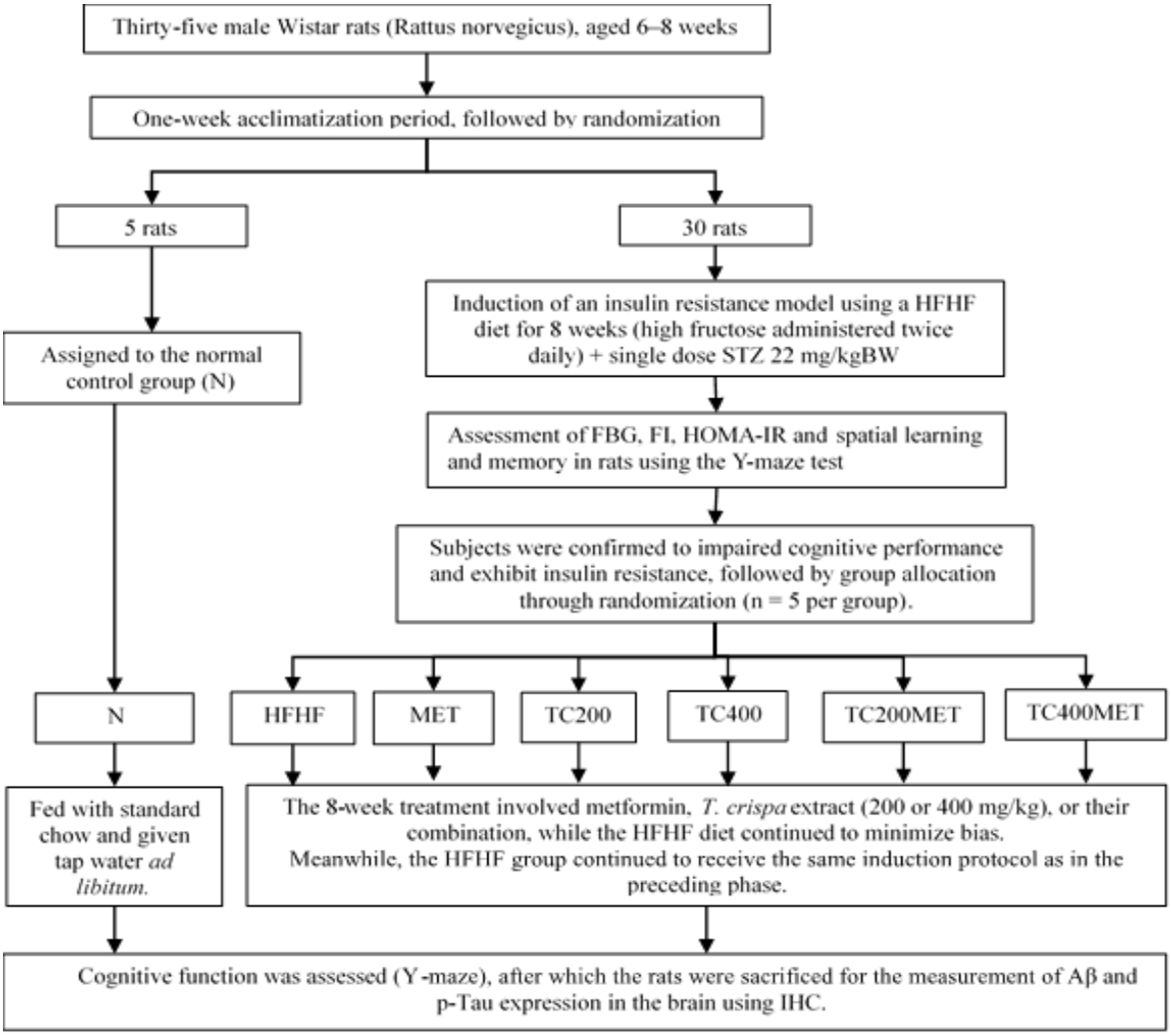

Figure 1. Experimental protocol diagram

Table 1. Experimental groups

Group names	Description
N	Normal control group
HFHF	HFHF-induced group without treatment (negative control)
MET	Metformin-treated group
TC200	Monotherapy with *T. crispa* extract at 200 mg/kgBW
TC400	Monotherapy with *T. crispa* extract at 400 mg/kgBW
TC200MET	Combination of *T. crispa* 200 mg/kgBW and metformin
TC400MET	Combination of *T. crispa* 400 mg/kgBW and metformin

Results

Prior to treatment allocation, insulin-resistant animals exhibited fasting glucose levels ranging from 148–172 mg/dl, fasting insulin levels of 0.61–0.84 ng/ml, and HOMA-IR values of 5.22–8.38, consistent with previously reported data (Rahma et al. 2026). These measurements confirm that all animals in the HFHF group developed comparable insulin resistance after 8 weeks of HFHF diet induction followed by a single dose of STZ, prior to intervention.

Attenuation of Aβ deposition in the rat hippocampus and cortex

The results of IHC staining of the hippocampus and cortex using anti–Aβ (1-42) are presented in Figures 2 and 3. Clear deposition of Aβ was observed in both the hippocampus and cortex following HFHF+STZ administration. This was characterized by brown staining localized around the neuronal nucleus within the cytoplasm along the CA1 region of the hippocampus in HFHF group (Figure 2A). The mean Aβ area in the HFHF group was 6.83 ± 1.55%, which was significantly higher than that in the N group (0.53 ± 0.04%; $p<0.0001$) (Figures 2A-B). Treatment with metformin significantly reduced Aβ plaque compared with the HFHF group. Interestingly, the TC200, TC400 and TC400MET groups showed greater reductions in Aβ deposition, with values approaching those of the N group ($p<0.0001$ vs HFHF), compared with MET and TC200MET ($p<0.01$ and $p<0.001$ vs HFHF, respectively).

This phenomenon was also evident in sections of the cortex. Brown staining within the neuronal cytoplasm indicated Aβ deposition which was markedly increased in the HFHF group compared with the N group ($p<0.0001$; Figure 3A). These findings are consistent with the observed reduction of hippocampal Aβ pathology following treatment. Administration of metformin, *T. crispa* at 400 mg/kg, and their combination significantly decreased cortical Aβ accumulation. Notably, the TC400 group exhibited the most pronounced reduction ($p<0.0001$ vs. HFHF) (Figure 3B).

Reduction of p-Tau expression only in the cortex of rat brain

Immunohistochemical analysis of the cortex with the anti-p-Tau (Thr231) antibody revealed distinct group differences (Figure 4). In the normal (N) group, Tau protein displayed the expected labeling pattern, localized within the cytoplasmic layer surrounding the neuronal nucleus. By contrast, the HFHF group exhibited intense p-Tau (Thr231) staining, present both in neuronal cell bodies and along nerve fibers, reflecting abnormal Tau distribution that likely indicates microtubule destabilization and impaired neuronal integrity (Figure 4A). A similar pattern was also observed in the TC200, TC200MET, and TC400MET groups. Conversely, rats treated with either metformin (MET) or the higher dose of *T. crispa* (TC400) demonstrated a marked reduction in p-Tau levels compared with the HFHF group ($p<0.05$ and $p<0.01$, respectively; Figure 4A-B), highlighting their protective role against Tau pathology. Meanwhile, the results of the p-Tau analysis in the hippocampus are not reported, as no Tau hyperphosphorylation was observed in either the N group, the HFHF group, or any of the treatment groups.

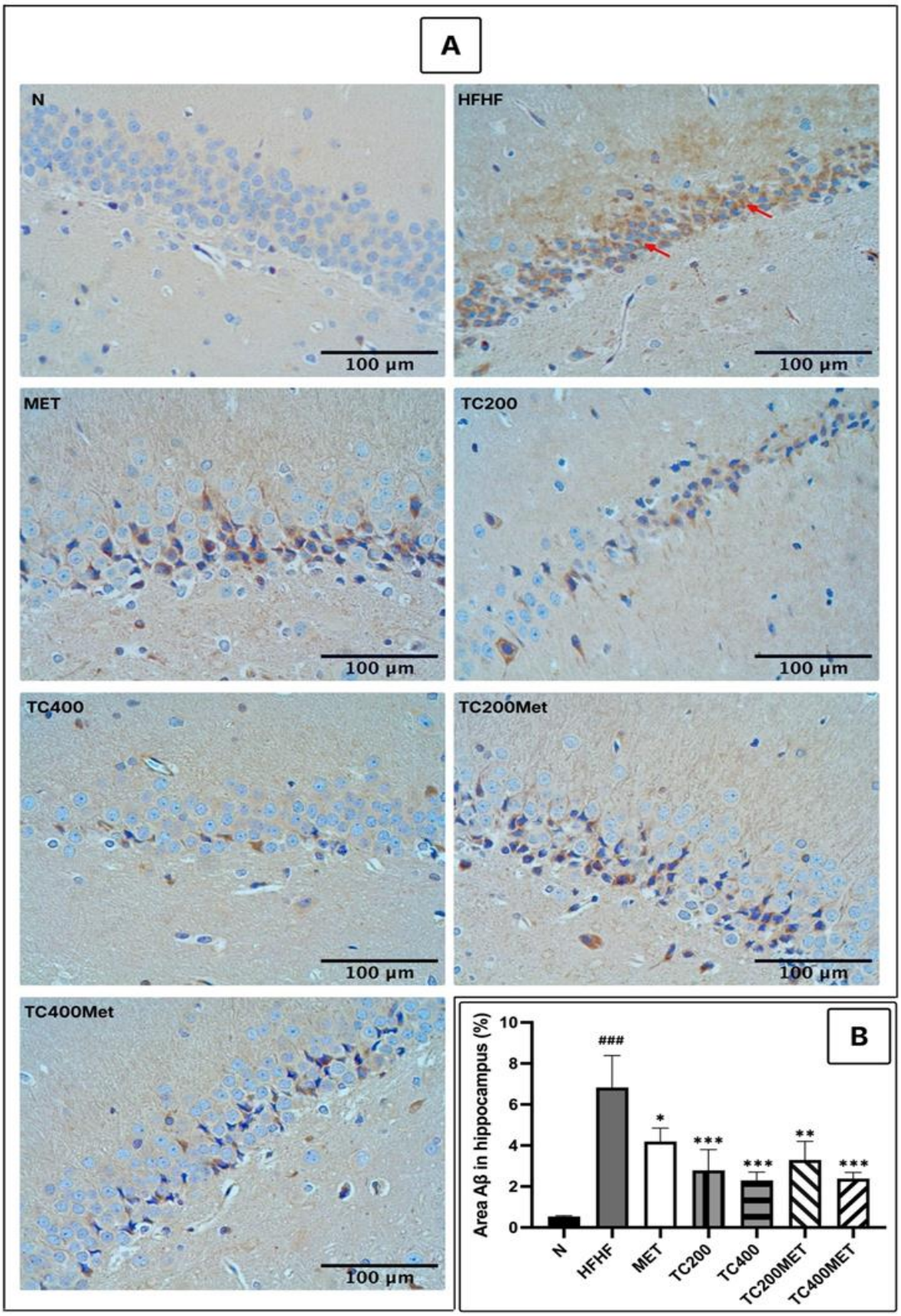

Figure 2. Deposition of Aβ in the hippocampus of rat brain. Differences in the appearance of Aβ plaque deposition (presence of brown color) in each group (A). Quantification of Aβ plaque area in the hippocampus **(**B**)**. Data are expressed as mean ± standard deviation. Magnification: 400x. ###p<0.0001 vs. N group; *p<0.01, **p<0.001 and ***p<0.0001 vs. HFHF group. Red arrows (→) indicate Aβ-positive staining.

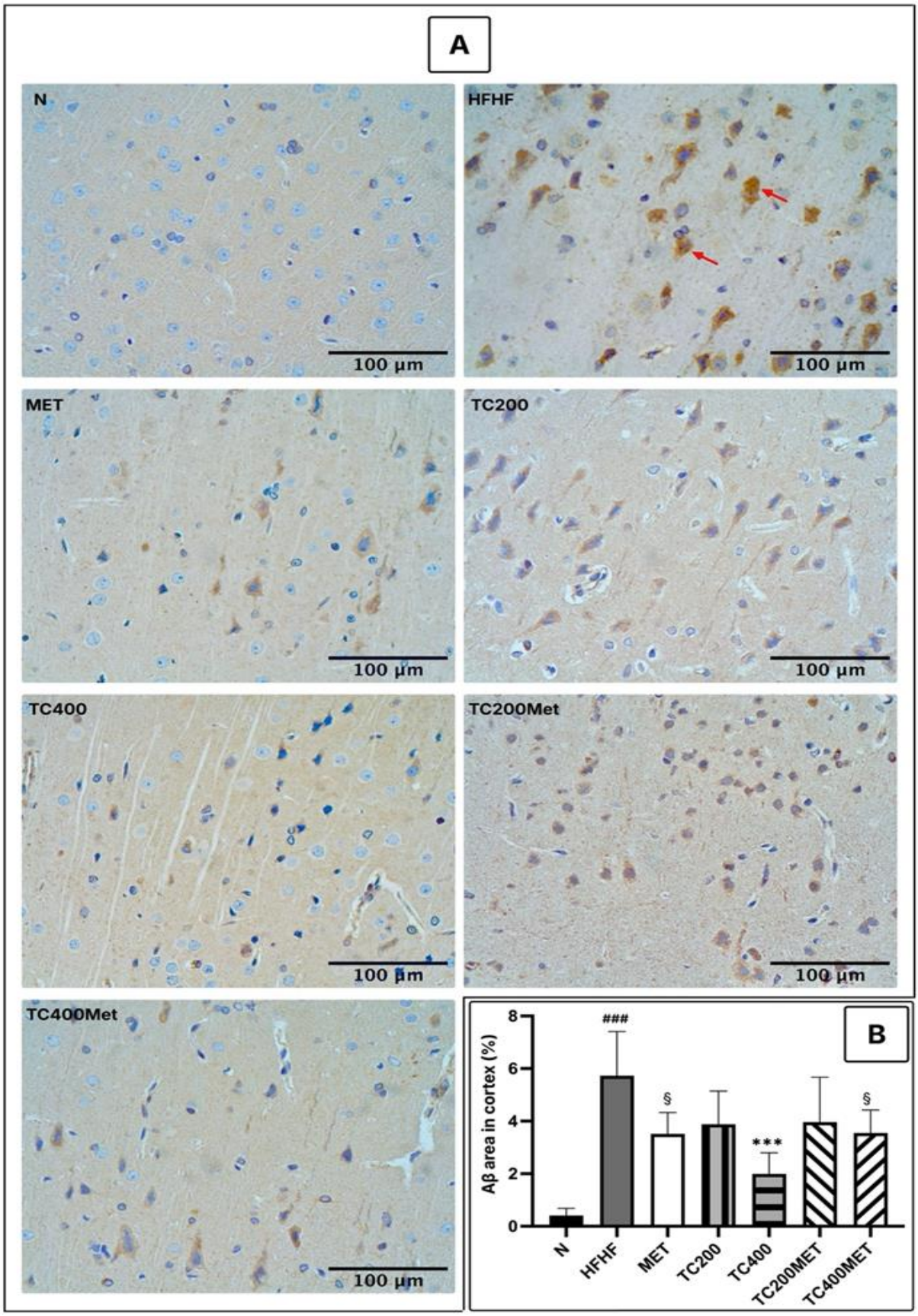

Figure 3. Deposition of Aβ in the cortex of rat brain. Differences in the appearance of Aβ plaque deposition (presence of brown color) in each group (A). Quantification of Aβ plaque area in the cortex **(**B**)**. Data are expressed as mean ± standard deviation. Magnification: 400x. ###p<0.0001 vs. N group; §p<0.05 and ***p<0.0001 vs. HFHF group. Red arrows (→) indicate Aβ-positive staining.

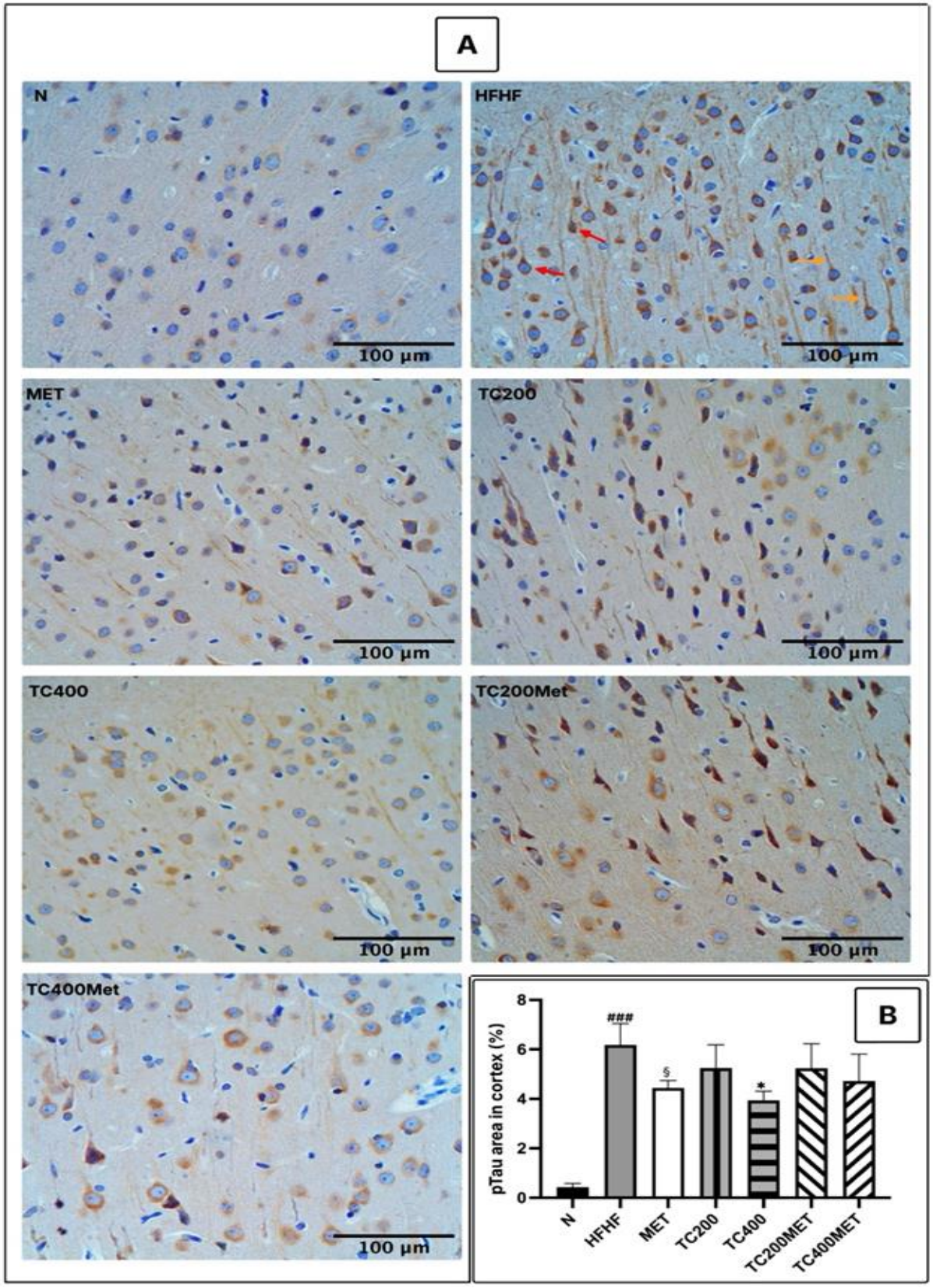

Figure 4. Representative microphotographs of p-Tau in the cortex of Wistar rat. The appearance of p-Tau in all treatment groups (A) was characterized by the presence of brown layers surrounding the nuclei and brownish nerve fibers. Quantification of p-Tau area in the cortex region **(**B**)**. Data are expressed as mean ± standard deviation. Magnification: 400x. ###p<0.0001 vs. N group; §p<0.05 and *p<0.01 vs. HFHF group. Red arrows (→) indicate p-Tau–positive staining in neuronal cell bodies; orange arrows (→) indicate p-Tau–positive staining in nerve fibers.

Effect of *T. crispa* extract on spatial and cognitive memory in rats

As baseline data, the initial SPA of rats at the beginning of the study was 71.79 ± 4.62%. After 8 weeks of HFHF diet feeding, the percentage of SPA declined significantly compared to the N group ($p<0.001$; Figure 5A). The findings from this study demonstrated that HFHF combined with STZ induction successfully impaired spatial and working memory, as reflected by the significant reduction in SPA in the Y-maze test. At the end of the study, prior to termination, spatial and memory function was reassessed (Figure 5B). Statistical analysis showed that the HFHF group exhibited a marked reduction in SPA (26.49 ± 16.10%) compared to the N group (72.35 ± 7.85%; $p<0.001$). The greatest improvement was observed in the TC400 group ($p<0.001$), while the MET group alone showed no significant difference compared with the HFHF group.

Correlation of cognitive decline with the emergence of Aβ and Tau hyperphosphorylation

Pearson correlation analysis revealed a strong negative association between spontaneous alternation performance and Aβ levels in the hippocampus ($r = –0.7970$, $p<0.0001$). A moderate negative correlation was also observed in the cortex ($r = –0.5068$, $p=0.0059$) (Figure 6A-B). In addition, spontaneous alternation was moderately and significantly correlated with p-Tau levels in the cortex ($r = –0.5142$, $p=0.0051$) (Figure 6C).

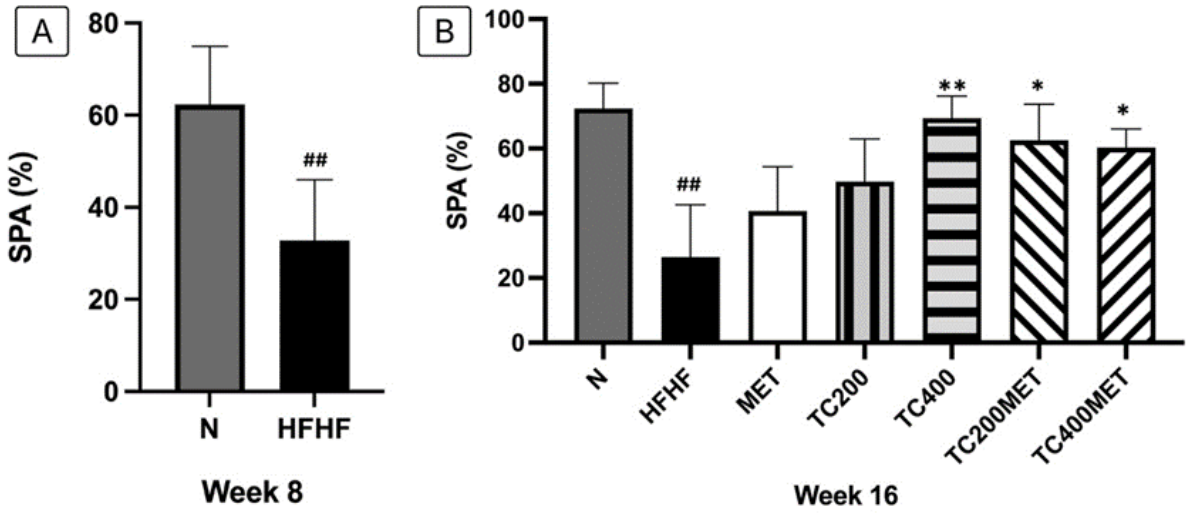

Figure 5. Percentage of SPA in rats as assessed using the Y-maze test. Measurements were performed at weeks 8 (A) and 16 (B). Data are expressed as mean ± standard deviation. ##$p<0.001$ vs. N group; *$p<0.01$, and **$p<0.001$ vs. HFHF group.

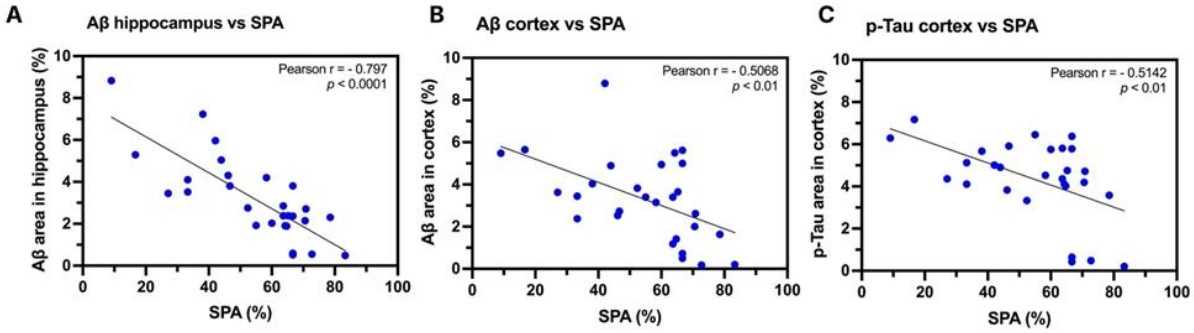

Figure 6. Correlation analysis of spontaneous alternation with Aβ deposition and p-Tau levels. Graph (A) shows the correlation between Aβ deposition and SPA in the hippocampus, graph (B) represents the correlation in the cortex, and graph (C) illustrates the correlation between p-Tau and SPA. All correlation analyses were performed using Pearson's test, with significance set at $p<0.05$.

In silico prediction results

Binding energies for all five tested compounds are summarized in Table S1. Among the tested compounds, borapetoside B and tinoscorside A demonstrated the highest binding affinities and, as the top performers, are the only compounds highlighted in the results. Detailed docking results indicated that these two major *T. crispa* constituents exhibited strong interactions with the amyloidogenic proteins BACE, PSEN1, and GSK3β (Table 2).

Both compounds demonstrated the most promising interactions when tested against Alzheimer's-related targets. Among the five tested ligands, the most stable interaction with BACE was observed for borapetoside B, showing a binding free energy of ΔG = –12.02 kcal/mol (Table 2). Previously, redocking of the native ligands yielded Root Mean Square Deviation (RMSD) values below 2 Å, indicating that the docking protocol reliably reproduced consistent binding poses and was suitable for further analysis (Table 3). Within this validated framework, *T. crispa* compounds showed more favorable binding energies (ΔG) and lower predicted inhibition constant (Ki) values than the native ligands, suggesting stronger and more competitive interactions with the target proteins involved in amyloid and Tau-related pathways.

PSEN1 exhibited strong binding with tinoscorside A, with a ΔG of –11.04 kcal/mol. In addition, tinoscorside A also emerged as the best ligand for GSK3β, with a binding free energy of ΔG = –10.36 kcal/mol. Notably, these interactions demonstrated both lower binding free energies and superior docking scores compared to metformin, underscoring their potential therapeutic relevance. The three best docking poses are illustrated in Figure 7. Together, these findings highlight their potential roles in modulating multiple pathological pathways central to AD progression.

Table 2. Molecular docking analysis of BACE, PSEN1, and GSK3β with the best ligand and metformin

Protein	Compound	ΔG (kcal/mol)	Ki (μM)	Interaction
BACE	Borapetoside B	-12.02	0.001	LEU30, TYR71, THR72, GLN73, PHE108, ILE110, TRP115, ILE118, THR231, THR232, ASN233, ARG235, ALA335
	Metformin	-6.55	15.72	ASP32, SER35, GLN73, ASP228, THR231
PSEN1	Tinoscorside A	-11.04	0.008	AL272, GLN276, LYS380, LEU381, THR421, LEU425, ALA431, ALA434
	Metformin	-5.35	119.58	ASP157, GLY382, ASP385
GSK3β	Tinoscorside A	-10.36	0.025	VAL70, LYS85, LEU132, VAL135, THR138, LYS183, GLN185, LEU188
	Metformin	-3.74	1830	ILE62, TYR134, ARG141

Table 3. Redocking results of target proteins with native ligands

Protein	Native ligand	IUPAC Name	ΔG (kcal/mol)	Ki (μM)	RMSD (Å)
BACE	BSD	(N-{(1S,2R)-1-benzyl-2-hydroxy-3-[(3-methoxybenzyl)amino]propyl}-5-[methyl(methylsulfonyl)amino]-N'-[(1R)-1-phenylethyl]benzene-1,3-dicarboxamide)	-12.97	308.88×10^{6}	1.93
PSEN1	ESF	((2S)-2-hydroxy-3-methyl-N-[(2S)-1-[[(5S)-3-methyl-4-oxo-2,5-dihydro-1H-3-benzazepin-5-yl]amino]-1-oxopropan-2-yl]butanamide)	-9.93	52.23×10^{3}	1.19
GSK3β	XV0	(2-(4-cyanoanilino)-N-(4-phenylpyridin-3-yl)pyrimidine-4-carboxamide)	-9.12	0.206	2.06

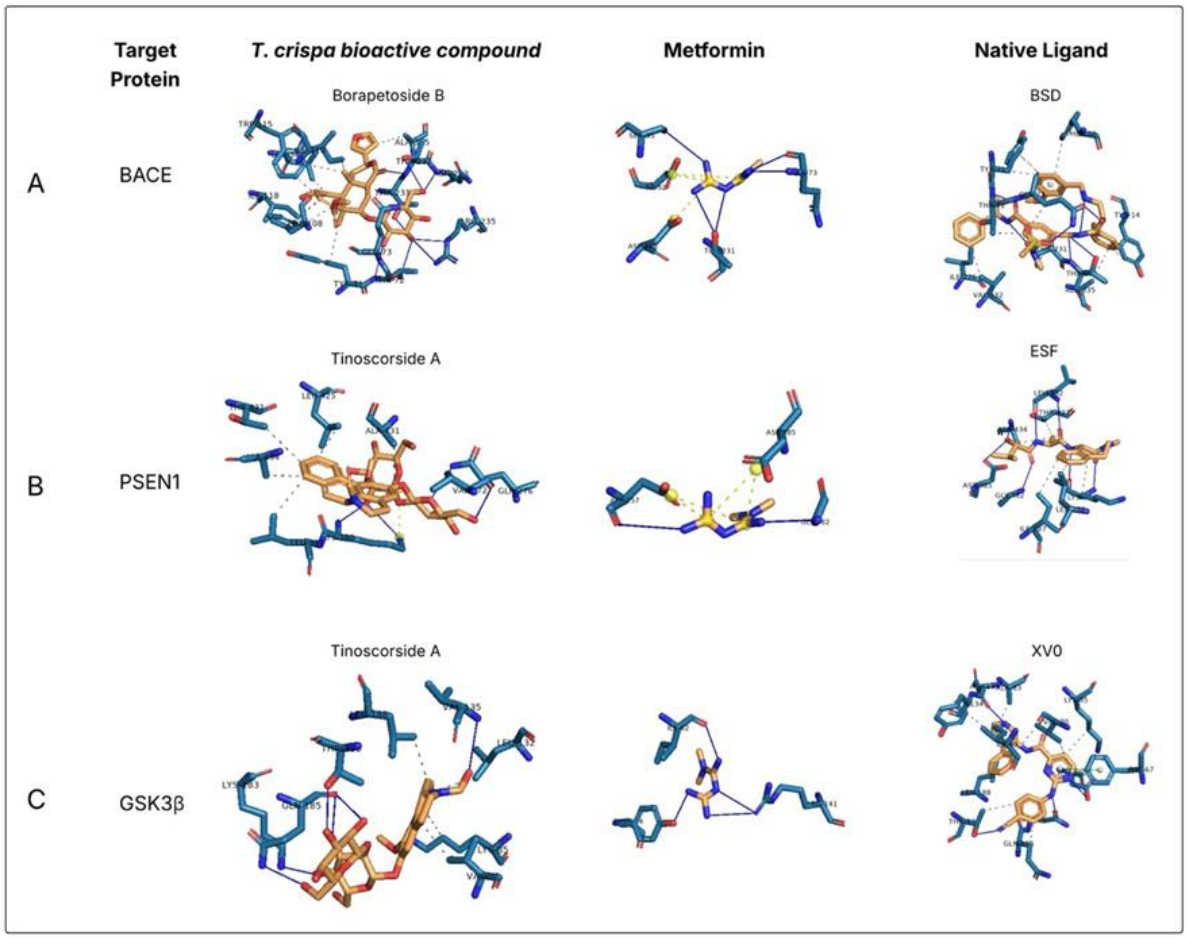

Figure 7. 2D visualization of molecular docking results. Three best molecular docking results: BACE (A) and borapetoside B, PSEN1 and tinoscorside A (B), and GSK3β and tinoscorside A (C).

Discussion

A high-fat, high-fructose (HFHF) diet combined with a single dose of STZ induces metabolic stress. This condition leads to neuronal system dysfunction, including Aβ accumulation and Tau hyperphosphorylation, which in turn impairs cognitive performance. In line with this pattern, Liang et al. reported similar outcomes (Liang et al. 2023), emphasizing the strong association between metabolic disturbances and neurodegenerative progression in AD. This work shows that Tau hyperphosphorylation occurs in the cortex, whereas the hippocampus remains largely unaffected, indicating a brain-region-specific response in the HFHF+STZ model. This finding is consistent with previous reports suggesting that the entorhinal cortex is more sensitive than the hippocampus to diet-induced brain insulin resistance and Alzheimer's-like molecular changes, even in wild-type animals without genetic modifications (Mietelska-Porowska et al. 2022). The molecular mechanisms leading to Tau hyperphosphorylation processes may therefore occur earlier in the entorhinal cortex than in the hippocampus, thereby explaining the absence of detectable hippocampal p-Tau in this study. These observations position HFHF diets as a significant risk factor and potential trigger for early Alzheimer's-type pathology and point to the need for interventions, such as dietary modification or metformin treatment, to target region-specific vulnerability within the brain.

Following eight weeks of metformin administration, this study confirms that metformin can reduce Aβ deposition and Tau hyperphosphorylation induced by the HFHF diet. This observation is consistent with prior studies showing that metformin

prevents amyloid plaque deposition and Tau hyperphosphorylation (Oliveira et al. 2021; Zhao et al. 2023), effects that are often accompanied by improved cognitive performance in experimental animals (Chellammal et al. 2022; Zhang et al. 2025). In contrast, the present study revealed a contrasting outcome. Metformin failed to improve spatial memory performance, as reflected by SPA results in the Y-maze. This lack of cognitive improvement is supported by findings reported by Cho et al., which showed that chronic metformin administration worsened memory outcome (Cho et al. 2024). Such inconsistencies may be attributed to the severity of HFHF-induced deficits or to side effects, such as vitamin B12 deficiency and mitochondrial inhibition, that may offset metformin neuroprotective effects (Farooq et al. 2022; Li et al. 2019; Yoval-Sánchez et al. 2022). Furthermore, the relatively short duration of treatment or the dosage used may have been insufficient to produce significant neuroprotective effects. Although metformin effectively improves peripheral insulin sensitivity, translating these effects to the brain—including the restoration of synaptic function and the cognitive improvement —likely requires a longer intervention period (Kodali et al. 2021; Rabieipoor et al. 2023).

Interestingly, *T. crispa* extract at a dose of 400 mg/kg produced the greatest improvement in spontaneous alternation performance ($p<0.001$), exceeding that observed with metformin monotherapy (Figure 5B). This finding is consistent with its effects in the hippocampus and cortex, which showed a more marked recovery through the suppression of Aβ plaque accumulation and Tau hyperphosphorylation. These results suggest that the neuroprotective potential is substantial, possibly comparable to or even greater than that of metformin alone. This evidence further supports the growing notion that safe, natural, plant-derived therapies deserve further mechanistic and translational exploration in AD models.

The superior efficacy of *T. crispa* may be attributed to its diterpenoid constituents, such as tinoscoroside A and brapetoside B (Zuhri et al. 2022), which modulate oxidative stress, promote neurogenesis, and support synaptic function (Gómez-Oliva et al. 2024; Salehi et al. 2023). Furthermore, *in silico* analyses revealed that BACE, PSEN1, and GSK3β exhibit much stronger interactions with borapetoside B or tinoscorside A than with metformin. This finding is noteworthy, given that dysregulation of these proteins is closely linked to amyloid plaque formation in AD. BACE acts as a rate-limiting enzyme in Aβ production, where altered glycosylation and misregulation exacerbate amyloid pathology (Hajdú et al. 2023). Likewise, PSEN1, the catalytic core of the γ-secretase complex, plays a central role in AD progression, with pathogenic variants accelerating amyloid deposition. Dysfunction of γ-secretase further increases Aβ42 accumulation and disrupts downstream signaling, thereby amplifying neurotoxicity (Gene at al. 2022; Zoltowska et al. 2024). In parallel, GSK3β activity promotes Tau hyperphosphorylation and aggregation into neurofibrillary tangles, further contributing to cognitive decline (Chakraborty et al. 2024).

This study is valuable as it addresses an important research gap by demonstrating that natural compounds from *T. crispa* can simultaneously inhibit all three major proteins—BACE, PSEN1, and GSK3β—implicated in AD (Figure 8). The proposed mechanism was developed using the Kyoto Encyclopedia of Genes and Genomes (KEGG) pathway map05010 (Alzheimer's disease) as a reference. The effects of *T. crispa* identified here were then integrated into this pathway to illustrate its potential involvement in amyloid-β formation and Tau hyperphosphorylation. Our findings suggest that the multitarget interaction of *T. crispa* constituents could offer a promising therapeutic approach that could

complement or possibly surpass the effects of single-target drugs, such as metformin.

In this context, the findings demonstrate that *T. crispa* at a dose of 400 mg/kg not only reproduces the beneficial actions of metformin but may also exert a greater effect on restoring normal Aβ and Tau regulation. This observation supports the potential of *T. crispa* as a candidate for preventing or slowing neurodegeneration.

A limitation of this study is the relatively small sample size per group (n = 5) and the absence of an a priori power analysis. The sample size was determined using Federer's formula for *in vivo* experiments and meets the recommended minimum. This approach also reflects standard practices in animal research that balance statistical rigor with ethical considerations. Nevertheless, the relatively small sample size may limit the detection of subtle effects. Future studies with larger sample sizes and formal power analyses are therefore needed to improve statistical power and confirm the observed effects.

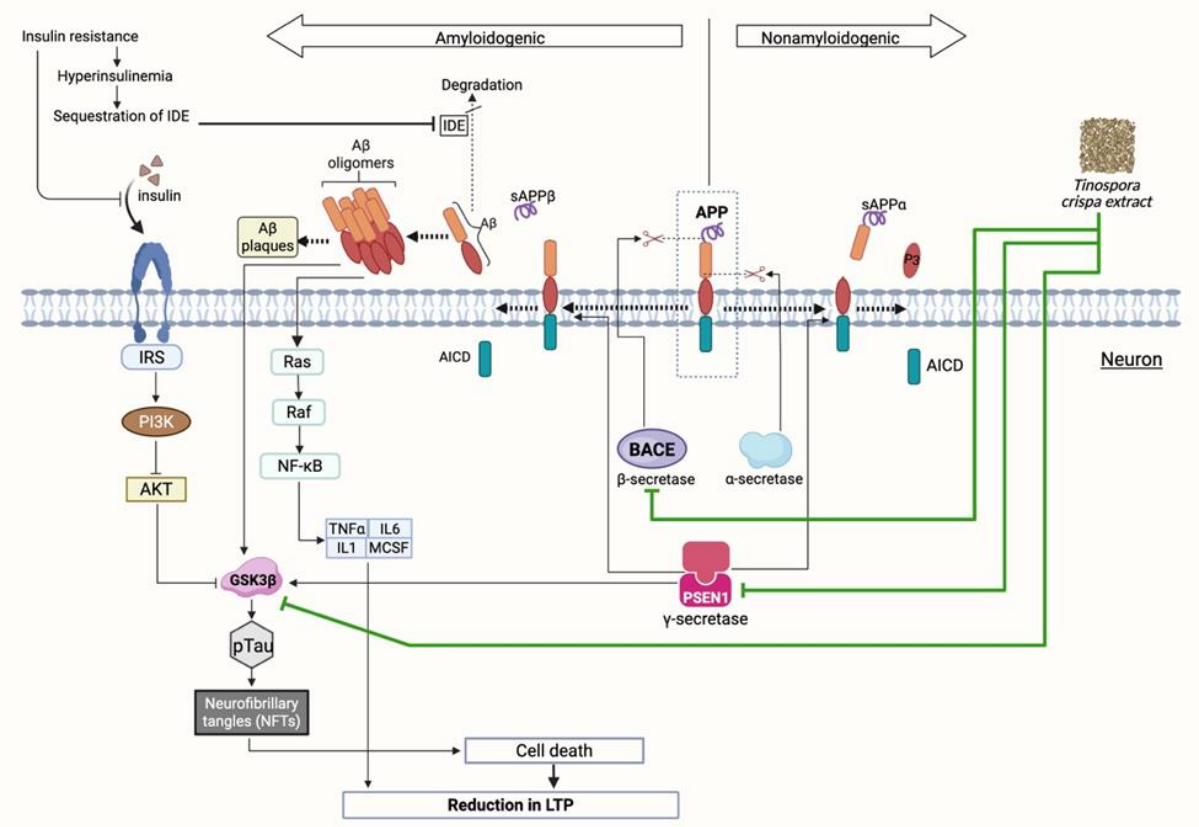

Figure 8. Proposed mechanism of *T. crispa* in Aβ Formation and Tau hyperphosphorylation in Alzheimer's disease. The role of *T. crispa* is marked with a green line.

Acknowledgment

The authors would like to express their sincere gratitude to the Faculty of Medicine, Universitas Indonesia, for their support in this study.

Conflicts of interest

The authors declare that they have no known competing financial interests or personal relationships that could have appeared to influence the work reported in this paper.

Funding

This work was financially supported by Universitas Indonesia (PUTI 2024 grant) [grant number NKB-259/UN2.RST/HKP.05.00/2024].

Ethical Considerations

All animal study protocols were approved by Health Research Ethics Committee of Dr. Cipto Mangunkusumo

Hospital – Faculty of Medicine, University of Indonesia, Jakarta, Indonesia.

Code of Ethics

Ethical approval no: (No. KET-1752/UN2.F1/ETIK/PPM.00.02/2023).

Authors' Contributions

KR: Conceptualization, Data curation, Formal analysis, Investigation, Methodology, Project administration, Resources, Software, Visualization, Writing – original draft. EHP: Conceptualization, Data curation, Funding acquisition, Methodology, Resources, Supervision, Validation, Visualization, Writing – review and editing. AA: Methodology, Supervision, Writing – review and editing. YR: Methodology, Supervision, Writing – review and editing. MK: Funding acquisition, Validation.

References

Ahmad W, Jantan I, Kumolosasi E, Bukhari SNA (2015) Immunostimulatory effects of the standardized extract of *Tinospora crispa* on innate immune responses in Wistar Kyoto rats. Drug Des Devel Ther 9: 2961–2973. doi:10.2147/DDDT.S85405

Akbarizadeh-Mashkani MH, Afshinmajd S, Iranzadeh S, Roghani M (2025) Involvement of synaptophysin and microtubule-associated protein 2 in the neuroprotective effect of berberine in an amyloid β-induced rat model of Alzheimer's disease. Avicenna J Phytomed 15(6): 1741–54. doi: 10.22038/ ajp.2025.26026

Chakraborty P, Ibáñez de Opakuab A, Purslowb JA, Frommc SA, Chatterjeeb D, Zachrdlab M, et al (2024) GSK3β phosphorylation catalyzes the aggregation of tau into Alzheimer's disease-like filaments. Proc Natl Acad Sci 121(52):e2414176121. doi:10.1073/pnas.2414176121

Chellammal HSJ, Hasan MH, Kshirsagar RP, Musukula VKR, Ramachandran D, Diwan PV (2022) Metformin inhibits cardiometabolic syndrome associated cognitive deficits in high fat diet rats. J Diabetes Metab Disord 21(2): 1415–1426. doi:10.1007/s40200-022-01074-4

Chen YK, Liu TT, Teia FKF, Xie FKF (2023) Exploring the underlying mechanisms of obesity and diabetes and the potential of traditional chinese medicine: An overview of the literature. Front Endocrinol 14: 1–18. doi:10.3389/fendo.2023.1218880

Cho SY, Kim EW, Park SJ, Phillips BU, Jeong J, Kim H, et al (2024) Reconsidering repurposing: long-term metformin treatment impairs cognition in Alzheimer's model mice. Transl Psychiatry 14: 34. doi:10.1038/s41398-024-02755-9

Diakité S, Mathurin M, Lhote F, Ngo S, Pasqualoni E, Versini E (2025) Lactic acidosis associated with metformin: a case series from the saint-denis hospital. Rev Med Interne 46(2): 68–73. doi:10.1016/j.revmed.2024.11.014

Farooq MD, Tak FA, Ara F, Rashid S, Mir IA (2022) Vitamin B12 deficiency and clinical neuropathy with metformin use in type 2 diabetes. J Xenobiot 12(2): 122–130. doi: 10.3390/jox12020011

Firdausa S, Cho MM, Maung KM, Aung N, Kuzaifah N, Suryawati N (2020) The blood glucose lowering effect of malaysian *Tinospora crispa* in rats. J Nat 20(1): 20–23. doi: 10.24815/jn.v20i1.15907

Gene P, Bagaria J, Bagyinszky E (2022) Genetics, functions, and clinical impact of presenilin-1. Int J Mol Sci 23: 10970. doi:10.3390/ ijms231810970

Gómez-Oliva R, Nunez-Abades P, Castro C (2024) New Pharmacological tools: The use of diterpenes to promote adult hippocampal neurogenesis. Neural Regen Res 19(8): 1629–1630. doi:10.4103/1673-5374.389635

Gunawan S, Munika E, Wulandari ET, Ferdinal F, Purwaningsih EH, Wuyung PE, et al (2023) 6-Gingerol ameliorates weight gain and insulin resistance in metabolic syndrome rats by regulating adipocytokines. Saudi Pharm J 31(3): 351–358. doi:10.1016/j.jsps.2023.01.003

Hajdú I, Végh BM, Szilágyi A, Závodszky P (2023) Beta-secretase 1 recruits amyloid-beta precursor protein to rock2 kinase, resulting in erroneous phosphorylation and beta-amyloid plaque formation. Int J Mol Sci 24:13. doi:10.3390/ijms241310416

Kim J, Kang H, Lee YB, Lee B, Lee D (2023). A quantitative analysis of spontaneous alternation behaviors on a y-maze reveals

adverse effects of acute social isolation on spatial working memory. Sci Rep 13(1):1477. doi:10.1038/s41598-023-41996-4

Knopman DS, Amieva H, Petersen RC, Chételat G, Holtzman DM, Hyman BT, et al 2021. Alzheimer disease. Nat Rev Dis Prim 7(1): 33. doi:10.1038/s41572-021-00269-y.

Kodali M, Attaluri S, Madhu LN, Shuai B, Upadhya R, Gonzalez JJ, et al (2021) Metformin treatment in late middle age improves cognitive function with alleviation of microglial activation and enhancement of autophagy in the hippocampus. Aging Cell 20(2): 1–19. doi: 10.1111/acel.13277

Kim SH, Park TS, Jin HY (2020) Metformin preserves peripheral nerve damage with comparable effects to alpha lipoic acid in streptozotocin/high-fat diet induced diabetic rats. Diabetes Metab J 45(1): 125–126. doi:10.4093/dmj.2019.0190

Li W, Chaudhari K, Shetty R, Winters A, Gao X, Hu Z, et al (2019) Metformin alters locomotor and cognitive function and brain metabolism in normoglycemic mice. Aging Dis 10(5): 949–963. doi:10.14336/AD.2019.0120

Liang Z, Gong X, Ye R, Zhao Y, Yu J, Zhao Y, et al (2023) Long-term high-fat diet consumption induces cognitive decline accompanied by tau hyper-phosphorylation and microglial activation in aging. Nutrients 15(1):250. doi:10.3390/nu15010250

Mietelska-Porowska A, Domanska J, Want A, Więckowska-Gacek A, Chutoranski D, Koperski M, et al (2022) Induction of brain insulin resistance and Alzheimer's molecular changes by western diet. Int J Mol Sci 23(9):4744. doi:10.3390/ijms23094744

Mobasher MA, El-Tantawi HG, El-Said KS (2020) Metformin ameliorates oxidative stress induced by diabetes mellitus and hepatocellular carcinoma in rats. Rep Biochem Mol Biol 9(1): 115–128. doi: 10.29252/rbmb.9.1.115

Mohamed HE, Asker ME, Younis NN, Shaheen MA, Eissa RG (2020) Modulation of brain insulin signaling in Alzheimer's disease: new insight on the protective role of green coffee bean extract. Nutr Neurosci 23(1): 27–36. doi: 10.1080/1028415X.2018.1468535

Mohammad HMF, Gouda SG, Eladl MA, Elkazaz AY, Elbayoumi KS, Farag KS, et al (2023) Metformin suppresses LRG1 and TGFβ1/ALK1-induced angiogenesis and protects against ultrastructural changes in rat diabetic nephropathy. Biomed Pharmacother 158:114128. doi: 10.1016/j.biopha.2022.114128

Nabrdalik K, Hendel M, Irlik K, Kwiendacz H, Łoniewski I, Bucci T, et al (2024) Gastrointestinal adverse events of metformin treatment in patients with type 2 diabetes mellitus: a systematic review and meta-analysis with meta-regression of observational studies. BMC Endocr Disord 24(1):206. doi: 10.1186/s12902-024-01727-w

Oliveira WH, Braga CF, Lós DB, Araújo SMR, França MR, Silva ED, et al (2021) Metformin prevents p-tau and amyloid plaque deposition and memory impairment in diabetic mice. Exp Brain Res 239(9): 2821–2839. doi: 10.1007/s00221-021-06176-8

Rabieipoor S, Zare M, Ettcheto M, Camins A, Javan M (2023) Metformin restores cognitive dysfunction and histopathological deficits in an animal model of sporadic Alzheimer's disease. Heliyon 9(7): e17873. doi:10.1016/j.heliyon.2023.e17873

Rahma K, Purwaningsih EH, Ramli Y, Aulanniam A (2026) Restoration of brain insulin signaling by *Tinospora crispa* extract via PI3K/AKT pathway modulation in HFHF-fed rats. Trends Sci 23(2): 11597. doi: 10.48048/tis.2026.11597

Salehi A, Ghanadian M, Zolfaghari B, Jassbi AR, P. Reisi, Csupor D, et al (2023) Neuropharmacological potential of diterpenoid alkaloids. Pharmaceuticals 16(5):747. doi: 10.3390/ph16050747

Shurrab NT, Arafa ESA (2020) Metformin: a review of its therapeutic efficacy and adverse effects. Obes Med 17:100186. doi: 10.1016/j.obmed.2020.100186.

Xu Y, Niu Y, Gao Y, Wang F, Qin W, Lu Y, et al (2017) Borapetoside E, a clerodane diterpenoid extracted from *Tinospora crispa*, improves hyperglycemia and hyperlipidemia in high-fat-diet-induced type 2 diabetes mice. J Nat Prod 80(8): 2319–2327.

doi: 10.1021/acs.jnatprod.7b00365
Yoval-Sánchez B, Ansari F, Lange D, Galkin A (2022) Effect of metformin on intact mitochondria from liver and brain: concept revisited. Eur J Pharmacol 931:175177. doi: 10.1016/j.ejphar.2022.175177
Zhang D, He X, Wang Y, Wang X, Han X, Liu H, et al (2025) Hesperetin-enhanced metformin to alleviate cognitive impairment via gut–brain axis in type 2 diabetes rats. Int J Mol Sci 26(5):1923. doi: 10.3390/ijms26051923
Zhao S, Fan Z, Zhang X, Li Z, Shen T. Li K, et al (2023) Metformin attenuates tau pathology in tau-seeded PS19 mice. Neurotherapeutics 20(2): 452–463. doi: 10.1007/s13311-022-01316-6
Zhao Y, Wang QY, Zeng LT, Weng JJ, Liu Z, Lin J, et al (2022) Long-term high-fat high-fructose diet induces type 2 diabetes in rats through oxidative stress. Nutrients 14(11):2181. doi: 10.3390/nu14112181
Zoltowska KM, Das U, Lismont S, Enzlein T, Maesako M, Houser MCQ, et al (2024) Alzheimer's disease linked Aβ42 exerts product feedback inhibition on γ-secretase impairing downstream cell signaling. ELife 12:RP90690. doi: 10.7554/eLife.90690
Zuhri UM, Purwaningsih EH, Fadilah F, Yuliana ND (2022) Network pharmacology integrated molecular dynamics reveals the bioactive compounds and potential targets of *Tinospora crispa* linn. as insulin sensitizer. PLoS ONE 17:e0251837. doi: 10.1371/journal.pone.0251837

Supplementary

Supplementary Table 1. Docking energies of five T. crispa compounds with target proteins.

Ligan	BACE		PSEN1		GSK3β	
	ΔG (kcal/mol)	Ki (μM)	ΔG (kcal/mol)	Ki (μM)	ΔG (kcal/mol)	Ki (μM)
Tinoscorside A	-11.46	0.003	-11.04	0.008	-10.36	0.025
Beta Sitosterol	-10.94	0.009	-10.08	0.04	-10.12	0.037
Borapetoside A	-8.74	0.394	-9.67	0.081	-8.43	0.658
Makisterone C	-8.46	0.634	-9.45	0.119	-7.7	2.28
Borapetoside B	-12.02	0.001	-8.26	0.826	-7.18	5.44
Metformin	-6.55	15.72	-5.35	119.58	-3.74	1830